Progress In Electromagnetics Research C, Vol. 172, 301–311, 2026
PIER C
(Received 18 June 2026, Accepted 29 July 2026, Scheduled 12 August 2026)

An Eight-Port MIMO Antenna with Broadband Self-Decoupling for 5G Applications

Xinxin Wang[1], Zhonggen Wang[1], Wenyan Nie[2,*], Shunqi Liu[1], and Quan Sun[3]

[1]*School of Electrical and Information Engineering, Anhui University of Science and Technology, Huainan 232001, China*
[2]*School of Mechanical and Electrical Engineering, Huainan Normal University, Huainan 232001, China*
[3]*School of Automation, Nanjing Institute of Technology, Nanjing 211167, China*

ABSTRACT: This paper proposes a polarization-orthogonal, self-decoupling, wideband, shared-radiator multiple-input multiple-output (MIMO) antenna for 5G mobile terminals. The antenna is fabricated on an FR4 dielectric substrate with a relative permittivity of 4.4 and a loss tangent of 0.02, and integrates a cross-shaped radiation patch, L-shaped slots, and metallized shorting vias into a 27 mm × 27 mm standard-sized substrate, and generates polarization-orthogonal modes through dual-port excitation, with an electrical size of $0.35\lambda_0 \times 0.35\lambda_0 \times 0.021\lambda_0$ at the center frequency of 3.9 GHz, which effectively suppresses the mutual coupling between ports. To fully demonstrate the wideband characteristics and self-decoupling advantages of this shared radiator, four identical antenna element pairs are arranged at the four corners of the smartphone rear cover, constructing an 8×8 MIMO antenna system operating in the 3.5–4.3 GHz frequency band. Simulated and measured results show that the proposed 8×8 MIMO system achieves an isolation better than 15 dB and an envelope correlation coefficient (ECC) less than 0.06. Featuring wideband operation and a passive self-decoupling structure, this antenna provides a promising design solution for 5G smartphone antennas.

1. INTRODUCTION

With the rapid development of the fifth-generation (5G) mobile communication technology, multiple-input multiple-output (MIMO) technology has become one of the core key technologies of 5G wireless systems [1–3]. However, achieving excellent MIMO performance in mobile terminals remains challenging. One major reason is that mutual coupling between MIMO antenna elements in the limited space of mobile terminals destroys the orthogonality of field distributions of different branches, resulting in the overlap of electromagnetic signals. This phenomenon increases channel correlation and significantly limits the system's channel capacity [4, 5]. Therefore, how to achieve efficient antenna decoupling under limited space constraints has become a critical problem that needs to be addressed in the current design of 5G terminal MIMO antennas.

The core challenge of 5G mobile terminal MIMO antennas lies in achieving multi-port integration, high isolation, and wideband coverage simultaneously within limited chassis space. Existing decoupling techniques fall into two categories: externally assisted decoupling and inherent self-decoupling. The former realizes isolation via additional structures, including defected ground structures (DGS) [6], decoupling networks [7], neutralization lines [8], and dedicated decoupling elements [9], but suffers from extra substrate space occupation, parasitic losses, and generally limited operating bandwidth. The latter suppresses inter-port mutual coupling by exploiting inherent isolation characteristics of antenna elements [10–17]. It delivers excellent port independence without auxiliary external components, making it highly suitable for space-constrained terminal scenarios. Among self-decoupling schemes, shared-radiator architectures with both wideband and high-isolation potential have drawn extensive research attention, forming representative technical routes such as polarization orthogonality [18–22], common-mode/differential-mode decoupling [23, 24], and lumped-element loading [25]. Nevertheless, most existing shared-radiator designs cannot simultaneously satisfy the multi-dimensional requirements of 5G mobile terminals for wideband coverage, high isolation, and high-density multi-port integration. In terms of terminal deployment configurations, existing designs can be further divided into centralized mainboard-edge layout and distributed four-corner layout. For mainboard-integrated schemes, the edge-arranged eight-element dual-polarized slot MIMO system proposed by Parchin et al. [26] achieves multi-port integration, but requires large edge clearance, is vulnerable to hand occlusion, and has limited spatial diversity gain and insufficient bandwidth. The dual-band four-port MIMO array developed by Elabd and Al-Gburi [27] improves isolation using additional decoupling structures, yet at the cost of higher circuit complexity and greater occupation of core mainboard space.

To address the above-mentioned research gap, this paper proposes a polarization-orthogonal shared-radiator antenna pair suitable for corner deployment in smartphones. With a distributed four-corner layout, an eight-port MIMO system is constructed and achieves wideband operation, high isolation, and excellent spatial diversity performance simultaneously without additional decoupling structures. By deploying two sets of symmetric feeding structures on the shared radiator, two groups

* Corresponding author: Wenyan Nie (wynie5240@163.com).

doi:10.2528/PIERC26061805

Published by THE ELECTROMAGNETIC ACADEMY

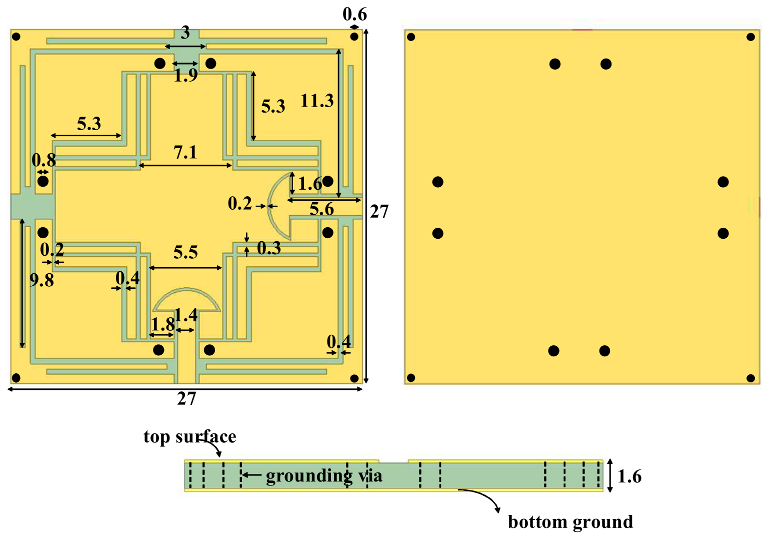

FIGURE 1. Geometry of the proposed antenna pair (unit: mm).

of dominant current modes with mutually orthogonal directions can be excited in the 3.5–4.3 GHz frequency band. Benefiting from the polarization-orthogonal self-decoupling characteristic, this dual-port antenna achieves an inherent isolation of more than 15 dB without requiring any additional external decoupling structures. The introduction of L-shaped slots and metallized shorting vias excites multiple resonant modes and effectively broadens the impedance bandwidth, which can basically cover the core 5G NR n77/n78 communication bands. Meanwhile, four identical antenna-element pairs are arranged at the four corners of the smartphone rear cover to construct an 8×8 MIMO antenna system. Both reliable simulated and measured results confirm that the proposed antenna array exhibits good impedance matching and isolation performance in the 3.5–4.3 GHz operating band. This design provides a promising, feasible solution for developing high-performance 5G/6G mobile terminal antennas in the future.

2. ANTENNA DESIGN AND ANALYSIS

2.1. Antenna Configuration

Figure 1 shows structural dimensions of the proposed shared-radiator antenna element pair. The antenna is fabricated on an FR4 dielectric substrate with a relative permittivity of 4.4 and a loss tangent of 0.02, and the overall dimension is 27 mm $\times$ 27 mm $\times$ 1.6 mm. The central cross-shaped metal patch constitutes the main radiating structure, and an L-shaped slot is etched into the cross-shaped metal patch. In addition, a square annular slot is introduced at the outer edge of the structure. Meanwhile, sixteen metallized shorting vias are placed at different positions of the antenna to further improve its performance.

2.2. Antenna Design Process

To elucidate the design concept of the proposed shared-radiator MIMO antenna pair, its evolution process is illustrated in Fig. 2. A centrally symmetric cross-shaped patch is designed as the primary radiating element, with folded square stubs symmetrically loaded at its four arm ends. This structure effectively bends the radiation path of the surface current and significantly increases its equivalent electrical length. This initial configuration only excites a single resonant mode, exhibiting a narrowband operating characteristic, covering 3.6–3.8 GHz with isolation better than 10 dB. Building upon Ant. 1, 12 metallized ground vias are symmetrically placed on the substrate to optimize the local current return paths. Meanwhile, two arc-shaped defected slots connected to their respective feed lines are etched on the right and lower arms of the cross-shaped radiator, which effectively improves the overall impedance-matching performance. After optimization, the proposed antenna achieves dual-band coverage of 3.55–3.75 GHz and 4.1–4.25 GHz with an isolation level of approximately 15 dB, and two distinct resonant peaks are observed in the S-parameter curves.

To further broaden the operating bandwidth of the proposed antenna, an L-shaped radiation slot is introduced inside the central cross-shaped radiator. By adjusting the length and position of the L-shaped slot, the two resonant modes are brought close to each other and superimposed, finally extending the antenna's impedance bandwidth to 3.5–4.3 GHz with stable isolation exceeding 15 dB across the entire bandwidth. This design fully covers the main portion of the 5G NR n78 frequency band (3.5–3.8 GHz) and further extends the operating range to 3.8–4.3 GHz.

2.3. Analysis of Self-Decoupling Mechanism and MIMO Comprehensive Performance

To further reveal the physical nature of the proposed antenna self-decoupling mechanism, this section conducts an in-depth analysis based on the orthogonality of ideal current distributions under different port excitations, as shown in Fig. 3. The excitation currents I_1 at Port 1 and I_2 at Port 2 are illustrated in the figure. When Port 1 is excited while Port 2 is terminated with a matched load, the dominant surface current component is distributed along the longitudinal direction, as shown in Fig. 3(a); when Port 2 is excited while Port 1 is terminated

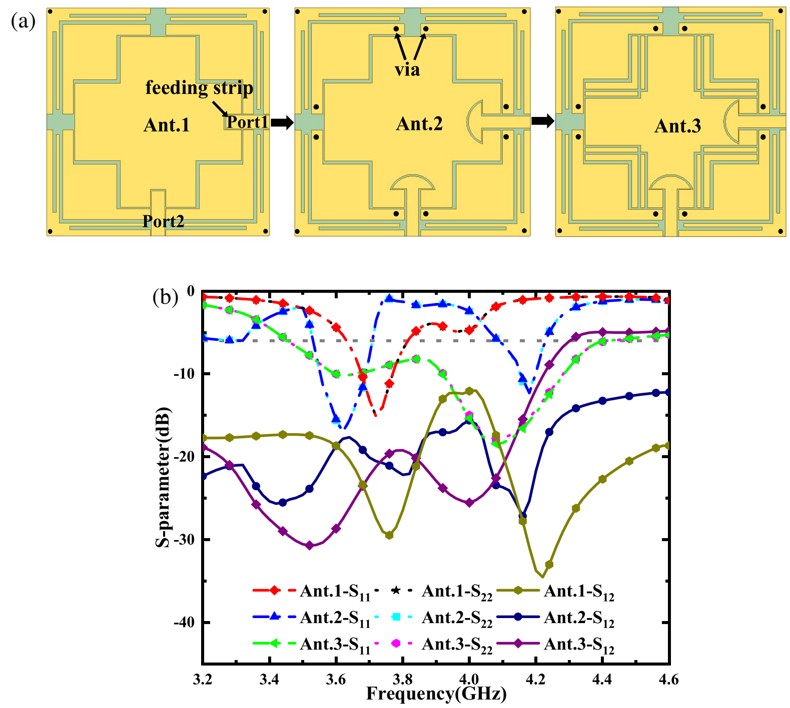

FIGURE 2. (a) Evolution process and (b) simulation results of the proposed two-port antenna.

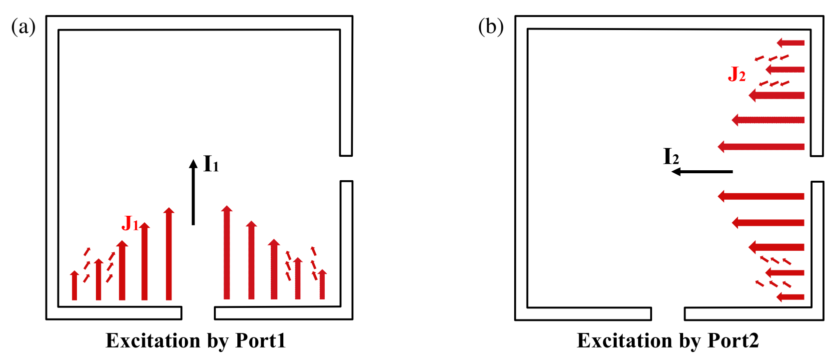

FIGURE 3. Theoretically excited current at different ports: (a) Port 1 and (b) Port 2.

with a matched load, the dominant surface current component is distributed along the transverse direction, as shown in Fig. 3(b). The surface currents under Port 1 and Port 2 excitations are decomposed into dominant current components and spurious current components, respectively (1):

$$\begin{aligned} I_1(x,y) &= J_1(x,y)\,\hat{x} + \Delta I_1(x,y) \\ I_2(x,y) &= J_2(x,y)\,\hat{y} + \Delta I_2(x,y) \end{aligned} \tag{1}$$

where $I_1(x,y)$ and $I_2(x,y)$ are the surface currents excited by the two ports, respectively; $J_1(x,y)$ and $J_2(x,y)$ represent the current amplitude distributions, respectively; x and y are the unit vectors in the transverse and longitudinal directions, respectively; ΔI_1 and ΔI_2 are the spurious currents in non-dominant directions, whose amplitudes are much smaller than those of the dominant current components.

By substituting the above current decomposition expressions into the mutual coupling integral formula, it can be derived that (2):

$$C = \iint_S \left[J_1\hat{x} + \Delta I_1\right] \cdot \left[J_2\hat{y} + \Delta I_2\right] dS \tag{2}$$

Expanding the aforementioned mutual coupling integral formula explicitly, we obtain (3):

$$C = \underbrace{\iint_S J_1 J_2 (\hat{x}\cdot\hat{y})\, dS}_{=0} + \underbrace{\iint_S J_1\hat{x}\cdot\Delta I_2 dS + \iint_S J_2\hat{y}\cdot\Delta I_1 dS + \iint_S \Delta I_1\cdot\Delta I_2 dS}_{C_{\text{residual}}} \tag{3}$$

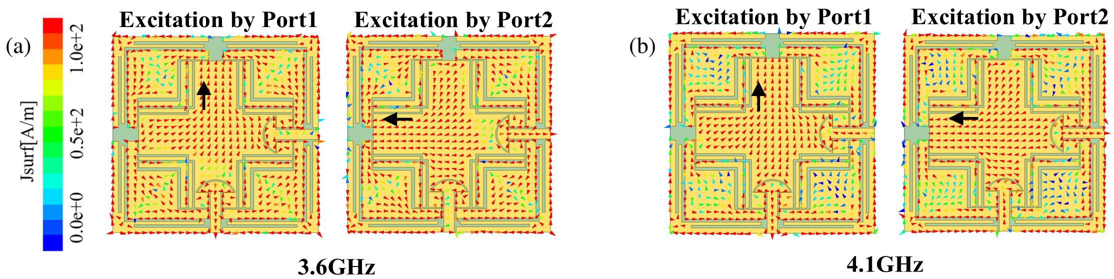

FIGURE 4. Surface current distribution at various angles: (a) 3.6 GHz and (b) 4.1 GHz.

The dominant current components are mutually orthogonal, so the coupling term is identically zero, which is the fundamental reason that the shared radiator achieves self-decoupling. The actual coupling only comes from the cross-coupling of spurious currents. Since the amplitude of spurious currents is very small, the system's mutual coupling level is extremely low, $C_{\text{residual}} \approx 0$. As the magnitudes of these spurious current components are orders of magnitude smaller than those of the dominant currents, the inter-port isolation is theoretically infinite.

To validate the aforementioned theoretical analysis, we investigate the simulated surface current distributions under different port excitations and radiation characteristics at representative operating frequencies. Fig. 4 depicts the surface current distributions for the two ports excited at 3.6 GHz and 4.1 GHz, respectively. As illustrated in Fig. 4, when the bottom port is excited, the dominant current flows predominantly along the longitudinal direction; conversely, when the right port is excited, the dominant current propagates primarily along the horizontal direction. Within the shared radiation region, the two ports excite two distinct sets of dominant surface currents with approximately orthogonal flow directions. Compared with the ideal current distribution, more spurious current components are observed, which accounts for the deviation from theoretical infinite isolation; nevertheless, the inter-port isolation remains consistently above 15 dB across the entire operating band. These results confirm that the proposed antenna achieves polarization orthogonality via the inherent orthogonality of dominant current directions, which enables stable self-decoupling performance.

Figure 5 presents radiation patterns of the dual-port shared-radiator, showing normalized simulated radiation patterns in the xoy and yoz planes at 3.6 GHz and 4.1 GHz. The simulated and measured data are in excellent agreement. The far-field distributions of the two ports exhibit significant orthogonality, and the orthogonal characteristic between xoy-plane radiation patterns directly verifies the polarization orthogonality of the shared radiator. This characteristic provides the physical basis for achieving high isolation (> 15 dB) within a compact spatial footprint.

Figure 6 presents multiple key performance characteristics of the proposed two-port shared-radiator MIMO antenna. Fig. 6(a) presents the total active reflection coefficient (TARC), which is less than -6 dB across the effective operating band, ensuring favorable impedance matching under simultaneous multi-port feeding; the diversity gain (DG) remains steadily above 9.8 dB, demonstrating outstanding anti-fading diversity performance. A MEG difference below 3 dB indicates good power balance among antenna ports, as shown in Fig. 6(b). In Fig. 6(c), the channel capacity loss (CCL) is kept below the threshold of 0.4 bit/s/Hz within the entire working bandwidth, which verifies weak mutual coupling and low channel correlation between the two ports. The peak gain curve in the third plot reveals that the antenna achieves a maximum peak gain of 2.6 dBi within the passband with stable radiation capability. All the above performance metrics satisfy the application specifications of MIMO antennas for 5G smartphone terminals.

2.4. Parametric Analysis

Figure 7 shows the parametric simulation study on the outer ring slot length, denoted by symbol c. As illustrated in Fig. 7, when the outer ring slot length c is reduced from 9.8 mm to 7.8 mm, the antenna's resonant frequency shifts toward lower frequencies, together with degraded port isolation. When c increases from 9.8 mm to 12.8 mm, the resonant frequency moves to higher frequencies, and both the impedance bandwidth and in-band isolation deteriorate. It can be concluded that the outer-ring slot length c can effectively tune the antenna's resonant characteristics. Considering the trade-off between bandwidth and isolation performance, $c = 9.8$ mm is selected as the optimal dimension.

3. SIMULATION AND MEASUREMENT RESULTS ANALYSIS

3.1. Results of the Eight-Element Antenna Array

Building upon the excellent performance of the shared-radiator dual-port antenna pair proposed in the previous section, this section extends it to an eight-port MIMO antenna system. Four identical antenna pairs are symmetrically deployed at the four corners of the smartphone rear cover, realizing an integrated multi-antenna design. Fig. 8(a) presents the three-dimensional topological structure and cross-sectional diagram of the eight-port MIMO system integrated on the smartphone rear cover. The system mainboard is fabricated on a standard FR-4 substrate with a thickness of 1.6 mm and overall dimensions of $150\,\text{mm}\times 75$ mm. To balance the array decoupling performance and terminal space utilization, the spacing between adjacent antenna pairs is set to 21 mm. This layout scheme not only fully

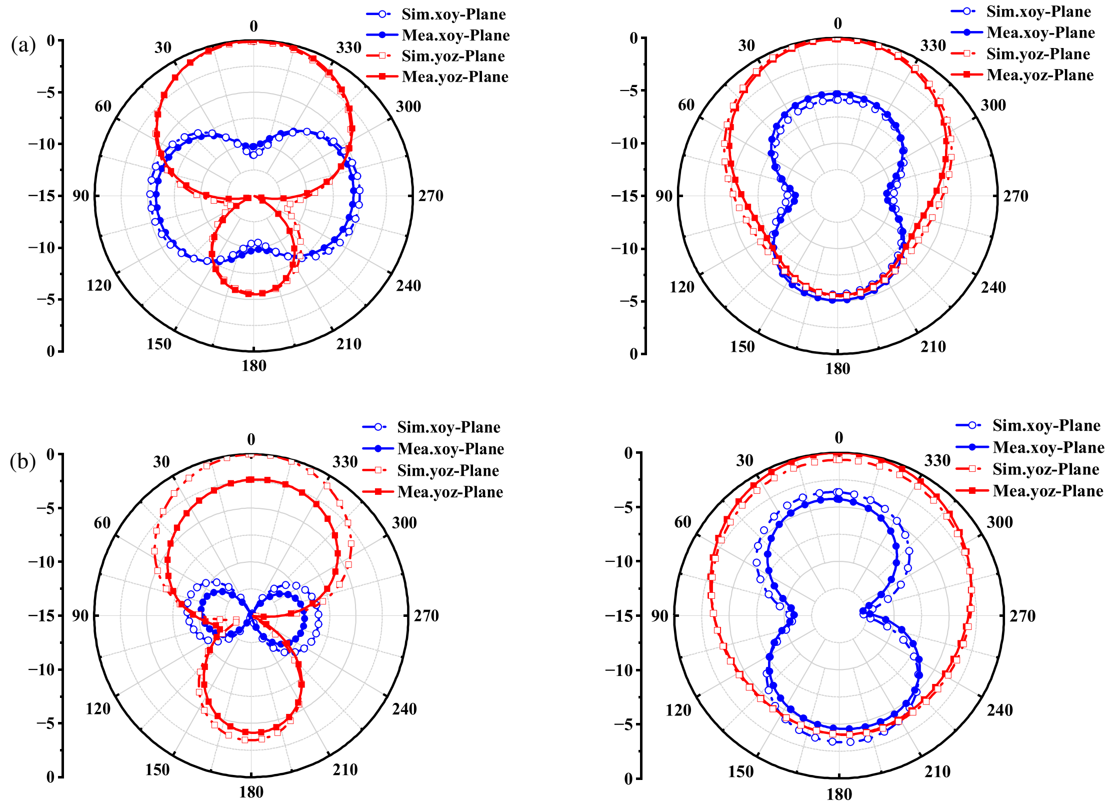

FIGURE 5. Dual-port simulated and measured radiation patterns in the xoy and yoz planes. (a) 3.6 GHz: Port 1 and Port 2. (b) 4.1 GHz: Port 1 and Port 2.

utilizes the unused space at the four corners of the terminal but also further reduces mutual coupling between array elements by increasing spacing between them.

To verify the feasibility and stability of the proposed eight-port MIMO system in practical complex electromagnetic environments, an antenna prototype is fabricated, and the antenna performance test platform built in a microwave anechoic chamber is shown in Fig. 8(b). The impedance characteristics and far-field radiation performance of each port are measured and analyzed in the experiment, aiming to verify the system's engineering practicability as a next-generation high-density mobile terminal communication architecture.

3.2. Antenna Array Performance: Simulation and Measurement

Figures 9(a) and 9(b) present the simulated and measured S-parameter results of the proposed eight-port MIMO antenna array. Owing to the array's excellent symmetry, representative ports are selected for analysis in this paper. As can be seen from Fig. 9(a), the simulated and measured reflection coefficients are in good overall agreement, with only minor deviations observed in isolation performance and frequency positions, indicating that the array can maintain stable impedance matching characteristics after fabrication. Meanwhile, the transmission coefficients between the two ports within the same shared-radiator element remain consistently low, demonstrating that the element-level polarization-orthogonal self-decoupling mechanism remains effective when extended to an eight-port array.

Figure 9(c) presents envelope correlation coefficient (ECC) and antenna efficiency results of the proposed eight-port MIMO antenna array. It can be observed that the ECC values in all representative port pairs remain low in the operating frequency band, generally below 0.06, indicating that the array has excellent spatial diversity. Meanwhile, the simulated and measured efficiency curves of representative ports are in good overall agreement and remain stable within the operating frequency band without significant efficiency degradation. The above results demonstrate that the proposed array maintains low channel correlation and stable radiation performance while achieving high-isolation integration, verifying its application potential in compact multi-port mobile terminal MIMO systems.

Figure 10 presents simulated and measured radiation patterns in the xoy and yoz planes at 3.6 GHz and 4.1 GHz. Owing to the structural symmetry of the array, only the test results of Port 1 and Port 2 are presented in this paper. As can be observed, the measured results are in good agreement with simulated ones. Compared with the radiation patterns of the dual-port shared-radiator antenna pair, those of the eight-port MIMO array exhibit a certain degree of pattern distortion. This is primarily attributed to mutual coupling between adjacent antenna elements and ports in the array. Nevertheless, the far-field radiation patterns of the two ports within each shared-radiator element still exhibit clear orthogonality, confirming that the polarization-orthogonal self-decoupling mechanism of the shared radiator is well preserved in the eight-port array.

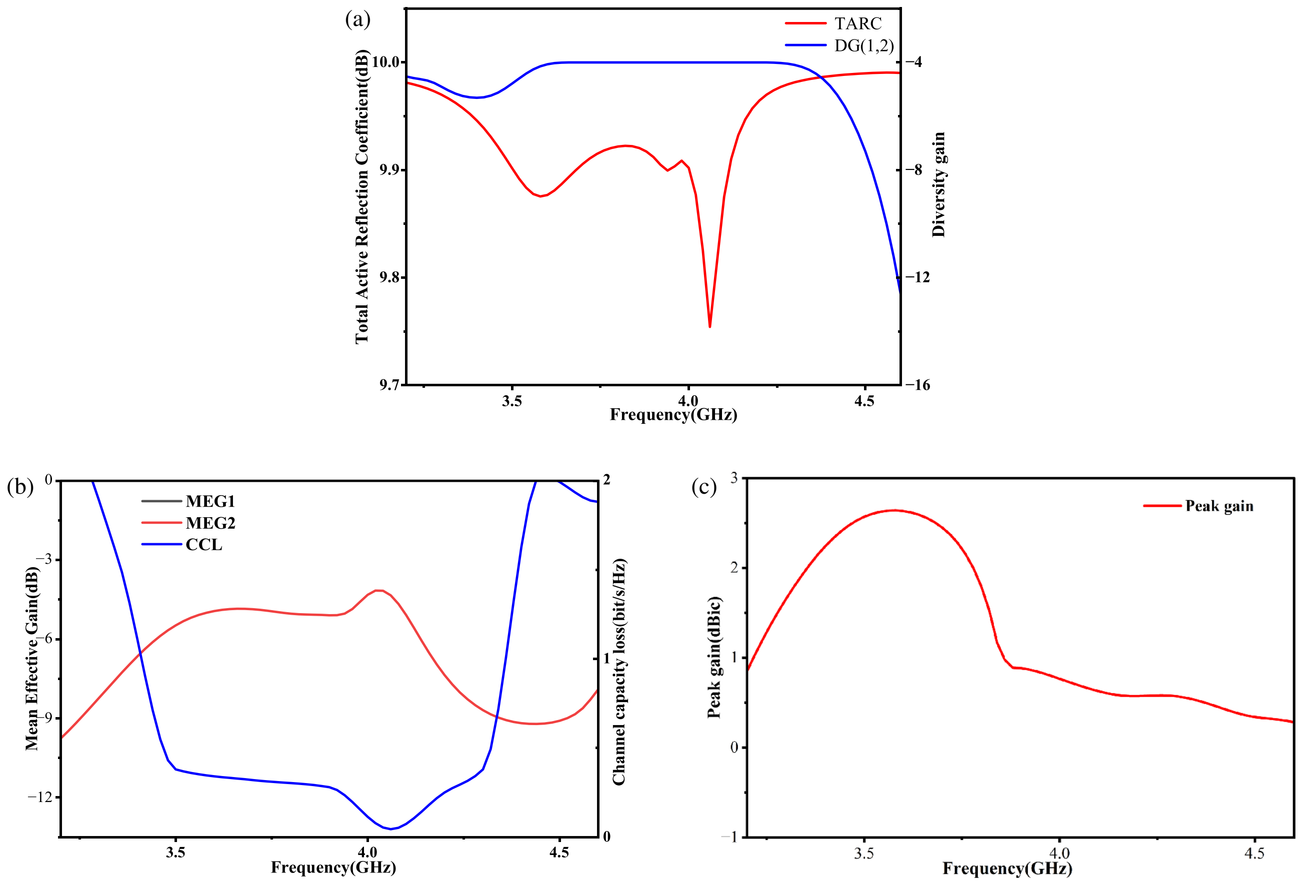

FIGURE 6. (a) TARC and DG, (b) MEG and CCL, and (c) peak gain.

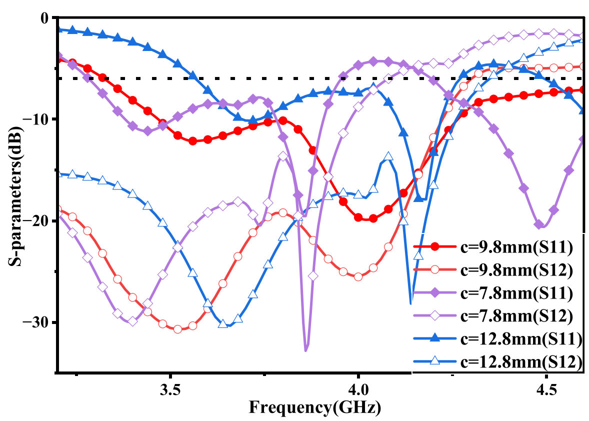

FIGURE 7. Parametric analysis of antenna performance with varying outer ring slot length c.

3.3. Application Scenario Analysis

To evaluate the practical performance of the proposed eight-port shared-radiator MIMO antenna for smartphone applications, full-wave simulations are carried out to analyze its specific absorption rate (SAR) and hand-loading effects. The analysis complies with the IEEE C95.1 standard, which specifies a limit of 1.6 W/kg for 1-g averaged SAR. With a maximum single-port input power of 23 dBm, the peak 1 g SAR reaches 1.57 W/kg within the operating band 3.5–4.3 GHz, which satisfies electromagnetic safety requirements. The SAR distribution on the smartphone back cover is illustrated in Fig. 11.

Figure 12(a) simulates the single-hand grip scenario. As shown in the simulation results for the typical single-hand operation in Fig. 12(b) and Fig. 12(c), matching and isolation performance degrade slightly due to the loading of human hand tissue; yet the antenna remains functional. Benefiting from the symmetrical four-corner layout and inherent polarization-orthogonal self-decoupling characteristics, the proposed antenna maintains stable performance under human tissue loading, demonstrating favorable engineering practicability for 5G mobile terminal applications.

3.4. Antenna Performance Comparison

Table 1 compares the proposed eight-port MIMO antenna with state-of-the-art 5G mobile terminal MIMO designs. For self-decoupling schemes, Refs. [28, 34, 35] achieve excellent isolation without additional structures but suffer from narrow bandwidths. Ref. [33] also adopts a structure-free self-decoupling architecture operating at 4.35–5.06 GHz with $>$ 15 dB isolation and $<$ 0.05 ECC; yet its total efficiency is only 40%–50%. For designs with extra decoupling structures, Ref. [36] delivers $>$ 17.5 dB isolation at the cost of external elements, but still has a narrow bandwidth and a high ECC of 0.23. Ref. [37] only achieves 12 dB moderate isolation. Refs. [29–32] real-

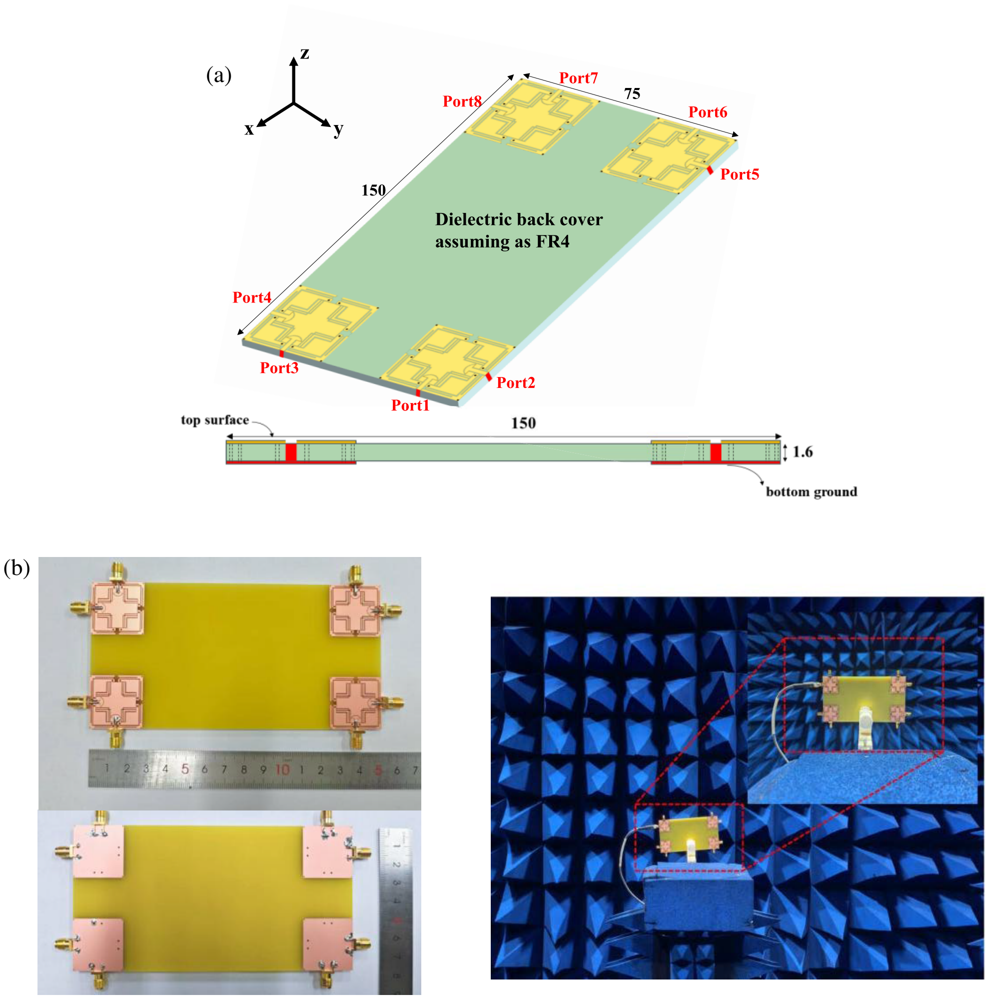

FIGURE 8. Configuration of the proposed 8 × 8 MIMO system. (a) Geometry of the proposed antenna array and (b) prototype photograph and anechoic chamber measurement.

TABLE 1. Antenna performance comparison.

References	Bandwidth (GHz)	Isolation (dB)	ECC	Total Efficiency (%)	Additional Decoupling Structure
[28]	3.4–3.6	> 16.7	< 0.1	54–65	No
[29]	4.25–5.13	> 12.5	< 0.15	50–57	Yes
[30]	4.4–6	> 10.5	< 0.32	41.6–71.9	Yes
[31]	5.13–5.84	> 12	< 0.23	51–74.3	Yes
[32]	3.3–6	> 12.1	< 0.2	50–61	Yes
[33]	4.35–5.06	> 15	< 0.05	40–50	No
[34]	3.3–3.8	> 20	< 0.14	40–70	No
[35]	3.4–3.6	> 17	< 0.065	60–75	No
[36]	3.4–3.6	> 17.5	< 0.23	51–74.3	Yes
[37]	3.4–3.6	> 12	< 0.05	59–73	No
Proposed	3.5–4.3	> 15	< 0.06	60–71	No

ize wide bandwidths, but their isolation falls below 13 dB with generally high ECC values, which fails to suppress crosstalk in high-density multi-port arrays. All of them also require auxiliary decoupling structures, further reducing integration density. In contrast, the proposed eight-port shared-radiator MIMO antenna attains port isolation greater than 15 dB, ECC smaller than 0.06, and total efficiency of 60%–71% over 3.5–4.3 GHz without additional decoupling structures, offering an extended

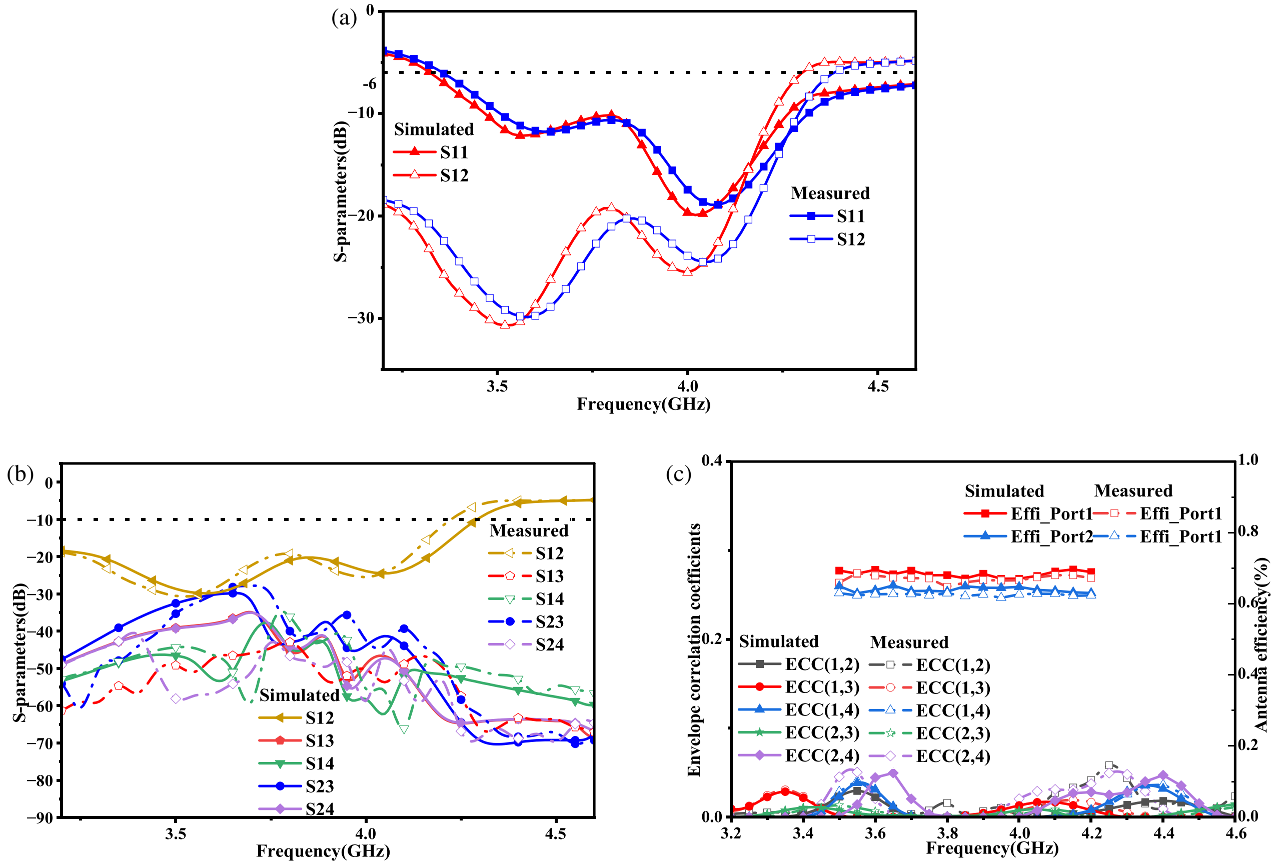

FIGURE 9. (a) Reflection coefficients, (b) transmission coefficients, and (c) ECCs and antenna efficiencies of the 8 × 8 MIMO system.

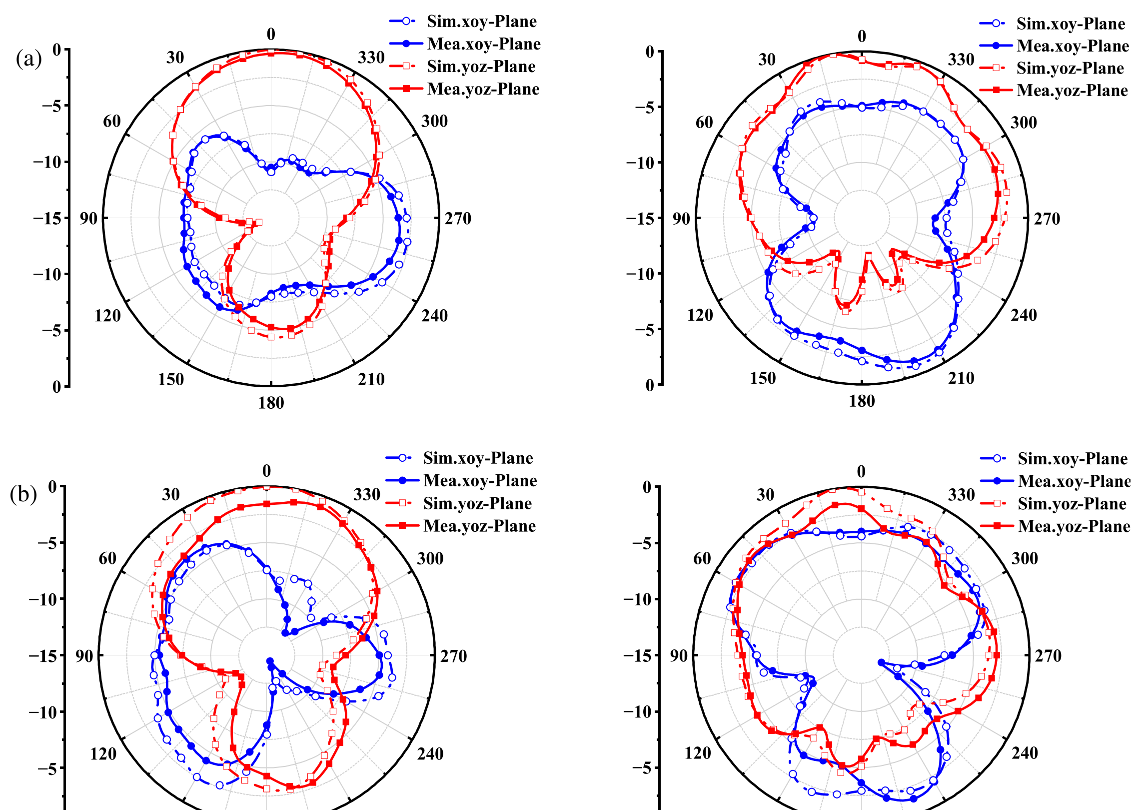

FIGURE 10. Eight-port simulated and measured radiation patterns in the xoy and yoz planes. (a) 3.6 GHz: Port 1 and Port 2. (b) 4.1 GHz: Port 1 and Port 2.

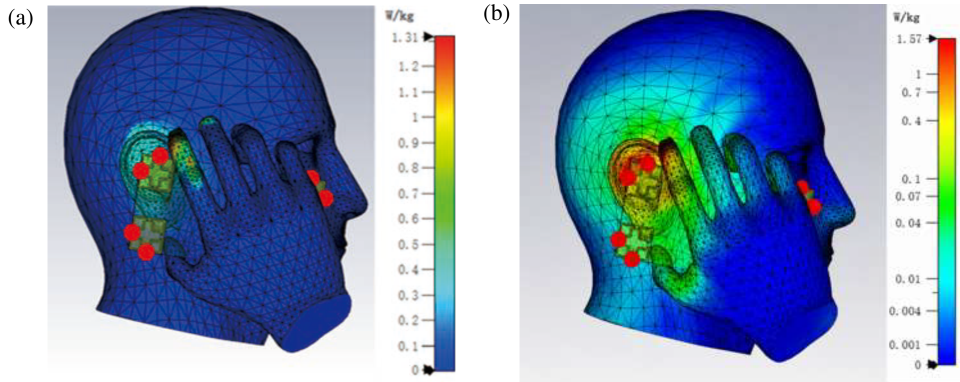

FIGURE 11. SAR analysis of the proposed MIMO antenna: (a) 3.5 GHz and (b) 4.1 GHz.

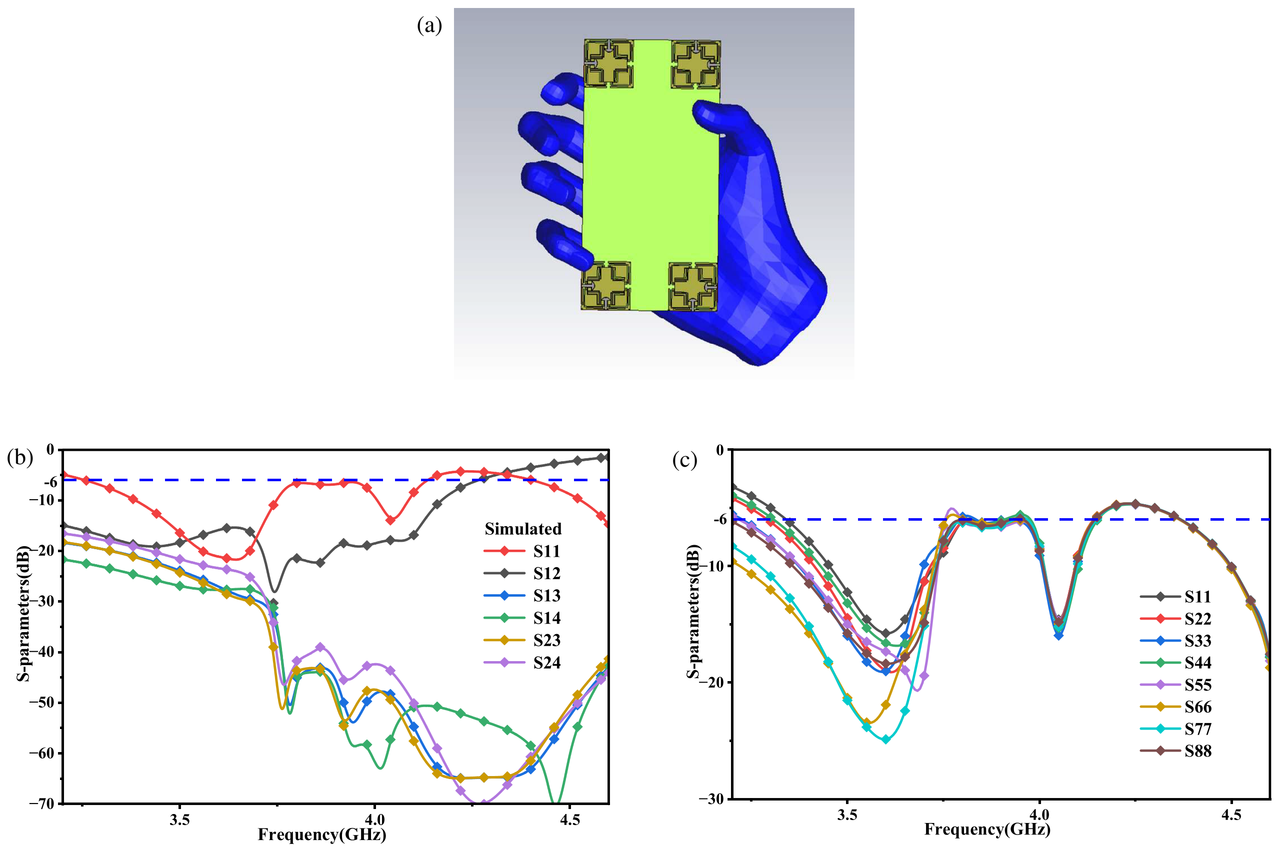

FIGURE 12. (a) Simulation model of hand loading effect and (b) corresponding simulation results.

bandwidth that fully covers the 5G NR n78 band. Its square geometry fits well for a four-corner symmetrical layout in smartphones, showing superior integration capability. Overall, this design strikes an optimal balance among bandwidth, isolation, ECC, efficiency, and integration, offering a competitive solution for high-density 5G smartphone MIMO applications.

4. CONCLUSION

This paper presents a wideband, eight-port polarization-orthogonal, self-decoupled MIMO antenna system based on the shared-radiator concept. This design uses the polarization-orthogonal self-decoupling mechanism, where mutually orthogonal surface current distributions are generated by exciting two orthogonal ports within the same shared-radiator element, thereby achieving high inter-port isolation without additional decoupling structures. Measured results demonstrate that the proposed eight-port MIMO system achieves port isolation greater than 15 dB and envelope correlation coefficient (ECC) less than 0.06 across the entire operating bandwidth of 3.5–4.3 GHz. This system simultaneously integrates wideband characteristics, high isolation, and polarization orthogonality, providing a promising solution for high-density 5G smartphone MIMO antenna design.

ACKNOWLEDGEMENT

This work was supported in part by the Natural Science Research Project of Anhui Educational Committee under Grant No. 2025AHGXZK31006, in part by the Research Foundation of Jiangsu Engineering Research Center for Bionics Control Technology and Equipment under No. FSKZ202503, and in part by the Anhui International Joint Research Center for Ancient Architecture Intelligence and Multi-Dimensional Modeling under No. GJZZX2025KF03.

REFERENCES

[1] Andrews, J. G., S. Buzzi, W. Choi, S. V. Hanly, A. Lozano, A. C. K. Soong, and J. C. Zhang, "What will 5G be?" *IEEE Journal on Selected Areas in Communications*, Vol. 32, No. 6, 1065–1082, Jun. 2014.

[2] Jungnickel, V., K. Manolakis, W. Zirwas, B. Panzner, V. Braun, M. Lossow, M. Sternad, R. Apelfröjd, and T. Svensson, "The role of small cells, coordinated multipoint, and massive MIMO in 5G," *IEEE Communications Magazine*, Vol. 52, No. 5, 44–51, May 2014.

[3] Boccardi, F., R. W. Heath, A. Lozano, T. L. Marzetta, and P. Popovski, "Five disruptive technology directions for 5G," *IEEE Communications Magazine*, Vol. 52, No. 2, 74–80, Feb. 2014.

[4] Kumar, A., K. Mishra, A. Mukherjee, and A. K. Chaudhary, "Channel capacity enhancement using MIMO technology," in *IEEE-International Conference on Advances in Engineering, Science and Management (ICAESM-2012)*, 10–15, Nagapattinam, India, Mar. 2012.

[5] Zhang, Z., *Antenna Design for Mobile Devices*, 2nd ed., John Wiley & Sons, Hoboken, NJ, USA, 2017.

[6] Chiu, C.-Y., C.-H. Cheng, R. D. Murch, and C. R. Rowell, "Reduction of mutual coupling between closely-packed antenna elements," *IEEE Transactions on Antennas and Propagation*, Vol. 55, No. 6, 1732–1738, Jun. 2007.

[7] Chen, S.-C., Y.-S. Wang, and S.-J. Chung, "A decoupling technique for increasing the port isolation between two strongly coupled antennas," *IEEE Transactions on Antennas and Propagation*, Vol. 56, No. 12, 3650–3658, Dec. 2008.

[8] Diallo, A., C. Luxey, P. L. Thuc, R. Staraj, and G. Kossiavas, "Study and reduction of the mutual coupling between two mobile phone PIFAs operating in the DCS1800 and UMTS bands," *IEEE Transactions on Antennas and Propagation*, Vol. 54, No. 11, 3063–3074, Nov. 2006.

[9] Mak, A. C. K., C. R. Rowell, and R. D. Murch, "Isolation enhancement between two closely packed antennas," *IEEE Transactions on Antennas and Propagation*, Vol. 56, No. 11, 3411–3419, Nov. 2008.

[10] Gao, S., L. W. Li, M. S. Leong, and T. S. Yeo, "A broad-band dual-polarized microstrip patch antenna with aperture coupling," *IEEE Transactions on Antennas and Propagation*, Vol. 51, No. 4, 898–900, Apr. 2003.

[11] Li, M.-Y., Y.-L. Ban, Z.-Q. Xu, G. Wu, C.-Y.-D. Sim, K. Kang, and Z.-F. Yu, "Eight-port orthogonally dual-polarized antenna array for 5G smartphone applications," *IEEE Transactions on Antennas and Propagation*, Vol. 64, No. 9, 3820–3830, Sep. 2016.

[12] Li, M.-Y., Y.-L. Ban, Z.-Q. Xu, J. Guo, and Z.-F. Yu, "Tri-polarized 12-antenna MIMO array for future 5G smartphone applications," *IEEE Access*, Vol. 6, 6160–6170, Dec. 2017.

[13] Li, W. W., B. Zhang, J. H. Zhou, and B. Q. You, "High isolation dual-port MIMO antenna," *Electronics Letters*, Vol. 49, No. 15, 919–921, Jul. 2013.

[14] Wang, H., Z. Zhang, and Z. Feng, "Dual-port planar MIMO antenna with ultra-high isolation and orthogonal radiation patterns," *Electronics Letters*, Vol. 51, No. 1, 7–8, Jan. 2015.

[15] Wen, D., Y. Hao, M. O. Munoz, H. Wang, and H. Zhou, "A compact and low-profile MIMO antenna using a miniature circular high-impedance surface for wearable applications," *IEEE Transactions on Antennas and Propagation*, Vol. 66, No. 1, 96–104, Jan. 2018.

[16] Ko, S. C. K. and R. D. Murch, "Compact integrated diversity antenna for wireless communications," *IEEE Transactions on Antennas and Propagation*, Vol. 49, No. 6, 954–960, Jun. 2001.

[17] Rao, Q. and D. Wang, "A compact dual-port diversity antenna for long-term evolution handheld devices," *IEEE Transactions on Vehicular Technology*, Vol. 59, No. 3, 1319–1329, Mar. 2010.

[18] Chang, L., Y. Yu, K. Wei, and H. Wang, "Orthogonally polarized dual antenna pair with high isolation and balanced high performance for 5G MIMO smartphone," *IEEE Transactions on Antennas and Propagation*, Vol. 68, No. 5, 3487–3495, May 2020.

[19] Li, M.-Y., Z.-Q. Xu, Y.-L. Ban, C.-Y.-D. Sim, and Z.-F. Yu, "Eight-port orthogonally dual-polarised MIMO antennas using loop structures for 5G smartphone," *IET Microwaves, Antennas & Propagation*, Vol. 11, No. 12, 1810–1816, Sep. 2017.

[20] Chang, L., Y. Yu, K. Wei, and H. Wang, "Polarization-orthogonal co-frequency dual antenna pair suitable for 5G MIMO smartphone with metallic bezels," *IEEE Transactions on Antennas and Propagation*, Vol. 67, No. 8, 5212–5220, Aug. 2019.

[21] Sun, L., Y. Li, Z. Zhang, and Z. Feng, "Wideband 5G MIMO antenna with integrated orthogonal-mode dual-antenna pairs for metal-rimmed smartphones," *IEEE Transactions on Antennas and Propagation*, Vol. 68, No. 4, 2494–2503, Apr. 2020.

[22] Xu, H., S. S. Gao, H. Zhou, H. Wang, and Y. Cheng, "A highly integrated MIMO antenna unit: Differential/common mode design," *IEEE Transactions on Antennas and Propagation*, Vol. 67, No. 11, 6724–6734, Nov. 2019.

[23] Sun, L., Y. Li, Z. Zhang, and H. Wang, "Self-decoupled MIMO antenna pair with shared radiator for 5G smartphones," *IEEE Transactions on Antennas and Propagation*, Vol. 68, No. 5, 3423–3432, May 2020.

[24] Ren, Z., A. Zhao, and S. Wu, "MIMO antenna with compact decoupled antenna pairs for 5G mobile terminals," *IEEE Antennas and Wireless Propagation Letters*, Vol. 18, No. 7, 1367–1371, Jul. 2019.

[25] Barani, I. R. R., K.-L. Wong, Y.-X. Zhang, and W.-Y. Li, "Low-profile wideband conjoined open-slot antennas fed by grounded coplanar waveguides for 4×4 5G MIMO operation," *IEEE Transactions on Antennas and Propagation*, Vol. 68, No. 4, 2646–2657, Apr. 2020.

[26] Parchin, N. O., Y. I. A. Al-Yasir, A. H. Ali, I. Elfergani, J. M. Noras, J. Rodriguez, and R. A. Abd-Alhameed, "Eight-element dual-polarized MIMO slot antenna system for 5G smartphone applications," *IEEE Access*, Vol. 7, 15 612–15 622, 2019.

[27] Elabd, R. H. and A. J. A. Al-Gburi, "Low mutual coupling miniaturized dual-band quad-port MIMO antenna array using decoupling structure for 5G smartphones," *Discover Applied Sciences*, Vol. 6, No. 4, 189, 2024.

[28] Fang, Y., Y. Jia, J.-Q. Zhu, Y. Liu, and J. An, "Self-decoupling, shared-aperture, eight-antenna MIMO array with MIMO-SAR reduction," *IEEE Transactions on Antennas and Propagation*, Vol. 72, No. 2, 1905–1910, Feb. 2024.

[29] Tian, X. and Z. Du, "Wideband shared-radiator four-element MIMO antenna module for 5G mobile terminals," *IEEE Trans-*

actions on Antennas and Propagation, Vol. 71, No. 6, 4799–4811, Jun. 2023.

[30] Ren, A., H. Yu, L. Yang, Z. Huang, Y. Liu, and J. Hou, "Massive 16-element wideband decoupled pairs with high integration for 5G smartphones," *IEEE Antennas and Wireless Propagation Letters*, Vol. 23, No. 12, 4114–4118, Dec. 2024.

[31] Tian, X., J. Wang, C. Zheng, and Z. Du, "Shared-radiator wideband grounded patch antenna pair with bending slot for mobile terminals," *IEEE Transactions on Antennas and Propagation*, Vol. 72, No. 4, 3724–3729, Apr. 2024.

[32] Ren, A., H. Yu, L. Yang, Z. Huang, Z. Zhang, and Y. Liu, "A broadband MIMO antenna based on multimodes for 5G smartphone applications," *IEEE Antennas and Wireless Propagation Letters*, Vol. 22, No. 7, 1642–1646, Jul. 2023.

[33] Zhang, S. and X.-M. Ni, "Compact shared-radiator four-element MIMO antenna module for 5G terminals," *Progress In Electromagnetics Research C*, Vol. 165, 284–290, Feb. 2026.

[34] Shao, R., X. Chen, J. Wang, and X. Wang, "Design and analysis of an eight-port dual-polarized high-efficiency shared-radiator MIMO antenna for 5G mobile devices," *Electronics*, Vol. 11, No. 10, 1628, May 2022.

[35] Hu, W., Z. Chen, L. Qian, L. Wen, Q. Luo, R. Xu, W. Jiang, and S. Gao, "Wideband back-cover antenna design using dual characteristic modes with high isolation for 5G MIMO smartphone," *IEEE Transactions on Antennas and Propagation*, Vol. 70, No. 7, 5254–5265, Jul. 2022.

[36] Moses, A. T. Z., N. Moses, and D. K. Janapala, "An electrically small 4-port self-decoupled MIMO antenna pairs operating in n78 5G NR band for smartphone applications," *AEU — International Journal of Electronics and Communications*, Vol. 145, 154082, Feb. 2022.

[37] Qu, L., H. Kim, K.-Y. Jung, and Y. Liu, "Compact four-port MIMO antenna module with decoupling components for 5G terminal devices," *IEEE Antennas and Wireless Propagation Letters*, Vol. 23, No. 7, 2224–2228, Jul. 2024.